**Supplemental Information for Partin et al., 2013**

## Site Location

The stalagmite was collected in November 2005 from Taurius Cave, Espiritu Santo, Vanuatu (15.5˚S, 167˚E). The cave is located near Narango Village at an elevation of ~230 m above sea level. The village sits on a plateau at the foot of a mountain range on the south, windward side of Santo. The southeast trades deliver moist air that provides mean annual rainfall of 2.5–3 m to the area with a strong seasonal maximum in DJF (Figure S1). As a result, a tropical forest grows above the cave. Pekoa Airport, the site where the modern rainfall record was measured (Figure 3), lies ~20 km east of the cave at an elevation of ~50 m above sea level. Pekoa Airport rainfall data is a compilation of NOAA GHCN data (http://www.ncdc.noaa.gov/ghcnm/) and data from the Vanuatu Meteorological and Geohazards Department (P. Masale, personal communication).

## Cave and Stalagmite Description

Taurius Cave is shaped like a narrow fissure ~2-8 m wide, 1-10 m high and ~400 meters long with a small stream along the bottom. A sinkhole located approximately halfway along the cave (200 m deep into the cave) that breaches the surface at a height of 30 m provides an estimate of the thickness of the overlying bedrock above the cave. A sump at the front entrance of the cave fills with water and blocks entry to the cave via the main entrance during the rainy season. The stalagmite sample grew halfway between the entrance and the sinkhole, or ~100 m from both

"entrances". The sample formed on a ledge approximately 5 m above the streambed. During a strong rainy season, the cave can partially flood for short periods, as evidenced by large sticks and small trees lodged on some of the upper ledges. The stalagmite, called "Big Taurius", is ~545 mm long (Figure S2). Brown layers in the sample (Figure S2) most likely indicate when rainfall was especially high and flooded the cave up to the 5 m ledge, which deposits a layer of mud on the surface of the stalagmite, as opposed to a hiatus in growth where the layer would represent dust collecting during desiccation. The brown layers correlate with more negative $\delta^{18}O$ values in the stalagmite supporting the notion that the brown layers represent flooding. Despite the white color of the sample (Figure S2), multiple analyses using powder X-ray diffraction (XRD) provide evidence that the stalagmite is >99% calcite. XRD scans show a large peak at a $2\theta$ of 29.4°, indicating calcite, and no intensity at the double peaks near 26°, indicating an absence of aragonite. Multiple analyses were measured at top, middle, and bottom of the stalagmite, as well as at peaks and troughs of $\delta^{18}O$ timeseries to test if a change in crystallography could cause the multi-decadal variability. All powder sub-samples were >99% calcite.

**Age Model**

Samples for U-Th dating were run on a Thermo-Finnigan "Neptune" multi-collector inductively coupled mass spectrometer (MC-ICP-MS) located at the National Taiwan University (Shen et al., 2012). Samples weigh between 150-700 mg, and the average analytical error is ~8 years ($2\sigma$). Age corrections were calculated using an estimated initial atomic $^{230}Th/^{232}Th$ ratio of 4 ± 2 ppm.

The age model for the sample is based on fitting quadratic splines to the U-Th dates (Figure S3). The median age model (dark curve) is based on the median U-Th ages and is the age model used to plot the timeseries in Figures 2-4. A Monte-Carlo approach is used to constructs alternative age models by allowing each U-Th date $t_i$ to vary according to a normal distribution with mean $\tau_i$ (its best estimate) and standard deviation $\sigma$ (its analytical uncertainty) over a $2\sigma$ range. All such 10,000 age models are plotted in Figure S3 in grey along with the median age model (the one assuming zero analytical error) in dark blue. The spread in the grey age models is a measure of the age uncertainty of each $\delta^{18}O$ measurement and is listed in the table with the raw data. For the spline fitting, we maximize the number of knots used to fit the quadratic splines, while not allowing for age inversions. By maximizing the number of knots, we target for the error between the spline fit and the U-Th ages to approximately equal the average analytical error. When the number of knots is allowed to arbitrarily increase, the spline fitting error decreases and the fit to the data improves, however this comes at the expense of generating age inversions. The 6 knots used here therefore represent a tradeoff between those two constraints. Matlab code is available upon request.

Pb-210 was determined via Po-210 by alpha spectrometry, and Po-209 was used as the yield determinant (Huh et al., 1990). Pb-210 dating of the upper portion of the stalagmite yields a growth rate of 0.7 mm/year (Figure S4), corroborating estimates from the U-Th age model.

**Stalagmite Isotopic Composition**

Stable isotopic samples were drilled at ~200 μm per sample for the upper 60 mm and ~355 μm for the rest of the sample on a computer-assisted micro-milling drilling system. A total of 1657 $\delta^{18}O$ analyses were measured on a Thermo-Finnigan MAT253 Isotope Ratio Mass Spectrometer (IRMS) or a Thermo-Finnigan Delta V Plus IRMS, with a Kiel IV Carbonate Device both at the Analytical Laboratory for Paleoclimate Studies (ALPS) at the Jackson School of Geosciences, University of Texas at Austin (repeat measurements of a carbonate standard has a long-term analytical precision of 0.12‰, 2σ). All stalagmite stable isotope values are reported relative to Vienna Pee Dee Belemnite (VPDB), in standard delta notation. The average temporal resolution is ~4 months per data point, and 98% of the age model has a temporal resolution less than or equal to 6 months. However, due to mixing in the overlying bedrock, the actual resolution of paleo-rainfall record is more than 4 months but less than 36, as some annual cyclicity is observed and is growth-rate dependent. Results from the $\delta^{13}C$ timeseries (Figure S5), Hendy tests (Hendy, 1971) (Figures S6 and S7) and modern cave dripwaters indicate that there is little evidence for kinetic effects (Mickler et al., 2004; Mickler et al., 2006; Dorale and Liu, 2009) controlling stalagmite $\delta^{18}O$ composition.

**Testing for Growth Rate and Sampling Resolution Bias in the Record**

Changes in the growth rate of the stalagmite and/or changes in the sampling resolution could possibly affect the amplitude of the multi-decadal stalagmite $\delta^{18}O$ shifts. Were changes in growth rate affecting the amplitude of the multi-decadal

variability, slower growth rates should result in smaller shifts, and vice versa. Growth rates at the bottom of the sample are similar to the top of the sample, on the order of 500-800 μm/year. At the bottom of the stalagmite where the growth rate is comparable to the top, the multi-decadal stalagmite $\delta^{18}O$ changes are much larger. For comparison, high growth rate segments (2-4 mm/year) in the middle of the stalagmite have multi-decadal shifts that that are both large and small in stalagmite $\delta^{18}O$. Therefore, we do not find a correlation between growth rate and the amplitude of the multi-decadal stalagmite $\delta^{18}O$ variability.

We tested the effect of sampling resolution on the variability of the stalagmite $\delta^{18}O$ record by generating two short isotopic records drilled along parallel transects on the upper 40 mm of the stalagmite, ~3 mm apart. One transect was sampled every 200 μm, whereas the other was sampled at every 355 μm. We note that this large change in sampling resolution does not change the amplitude of the multi-decadal signal in the slower growing, topmost part of the stalagmite, as the two $\delta^{18}O$ records are virtually identical. We report the higher resolution path (200 μm/sub-sample) for the upper portion of the record.

**Evaluation of Isotopic Equilibrium Precipitation of Calcite**

Results from the $\delta^{13}C$ timeseries (Figure S5), Hendy tests (Hendy, 1971) (Figures S6 and S7) and modern cave dripwaters indicate that there is little evidence for kinetic effects (Mickler et al., 2004; Mickler et al., 2006; Dorale and Liu, 2009) controlling stalagmite $\delta^{18}O$ composition. While a cross-plot of $\delta^{18}O$ vs. $\delta^{13}C$ shows that they

share 50% of their variance (Figure S6), comparison of the $\delta^{18}O$ (Figure 2a) and $\delta^{13}C$ (Figure S5) reveals that the shared variance is due to high frequency variability. The high frequency changes are due to the seasonal cycle of rainfall and interannual variability associated with ENSO – both of which are large perturbations to the local climate. The multi-decadal variability in the $\delta^{18}O$ timeseries is not present in the $\delta^{13}C$ timeseries, indicating rainfall variability is driving the changes in $\delta^{18}O$. Additionally in another version of the Hendy test, overlapping paths show no progressive enrichment from the center to the edge in $\delta^{18}O$ (Figure S7). Lastly, we collected cave dripwaters during a return visit to the cave in 2011. Given the cave temperature of ~25.5°C and $\delta^{18}O$ dripwater values from the cave of approximately -5‰ (VSMOW), conversion to calcite assuming isotopic equilibrium, and using an equation specifically for cave environments (Tremaine et al., 2011), yields a value of -5.8‰ (VPDB) – directly in line with values for the topmost portion of the stalagmite (Figure 2a).

**"Amount Effect" Conversion**

We base our conversion of stalagmite $\delta^{18}O$ to rainfall amount from modern stalagmite $\delta^{18}O$ and rainfall data on Espiritu Santo, Vanuatu. We choose to use 10-year decadal means to compare mean stalagmite $\delta^{18}O$ and rainfall amount between wet and dry periods (i.e. different PDV phases) (Figure S8). Dating errors preclude us from using a regression between stalagmite $\delta^{18}O$ and rainfall amount yearly data during the instrumental era. The slope of the regression yields a conversion of 1‰ stalagmite $\delta^{18}O$ per 1.4 m/wet season ($R^2 = 0.74$); an inverse correlation known as

the “Amount Effect” (Dansgaard, 1964; Rozanski et al., 1993). For example, the difference between the mean values of the 10-year epochs 1968-1977 and 1978-1987 yields a decrease of 0.48‰ of stalagmite $\delta^{18}O$, or an increase of 0.7 m/wet season. Troughs in both time series in 1930/1940 and 1980/1990 with a peak centered at c. 1960 indicate the ~50-year periodicity during the instrumental era, which is present throughout the entire stalagmite time series. For comparison, the difference between the epochs 1616-1625 and 1635-1644 yields an increase of 1.3‰, or decrease of 1.8 m/wet season. The amount effect conversion agrees with a modern study on Guam of 1.4 m/year of rainfall per 1‰ of amount weighted rainfall $\delta^{18}O$ (Partin et al., 2012). Guam is an appropriate site to compare to Vanuatu as both have similar mean annual and amplitude of seasonality of rainfall, although seasonality is 180 degrees out of phase due to their positions being in different hemispheres. Geochemically, the two sites are also similar as waters collected in 2011 from Vanuatu show similar cave dripwater $\delta^{18}O$ values, -5‰ (VSMOW), and dry season rainwater values, 0 to -1.5‰ (VSMOW), as in Guam.

**Historical Records of Drought**

Historical records of regional drought also support the interpretation that more positive stalagmite $\delta^{18}O$ values indicate drier conditions. In 1860 and c. 1866/67, droughts were recorded in the accounts of missionary, John G. Paton, when local Ni-Vanuatu people wanted to sacrifice him on two separate occasions as they thought Paton brought the drought to Vanuatu (Paton, 1893). These two droughts appear as two abrupt spikes towards more positive stalagmite $\delta^{18}O$ values. In the 1880’s (most

likely 1882), the capital was moved from Port Havannah on the north, leeward side of Efate Island to the south, windward side to Port Vila due to drought and malaria (MacClancy, 1981; The_Lonely_Planet, 2012), which also corresponds to a prolonged period of positive stalagmite $\delta^{18}O$ values.

**Karst Hydrologic Model**

We evaluate the effect of karst dynamics on the spectral characteristics of rainfall, as estimated from the $\delta^{18}O$ of calcite in the Big Taurius speleothem record. Because the hydrology of a real karst system involves flow through a complex geometry of fractures, our intent is not to replicate reality, but to offer a conceptual framework for quantifying the effects of aquifer dynamics on the isotopic signal recorded by the speleothem. A simple representation of such dynamics is via the box model of Gelhar and Wilson (Gelhar and Wilson, 1974). In this model, the authors find that the level of the aquifer $h$ can be represented very simply by the following ordinary differential equation:

$$\phi \frac{dh}{dt} + a(h - h_o) = f(t) \quad (1)$$

where $\phi$ is the average effective porosity of the aquifer, $a$ is an outflow constant, $h_o$ is a constant reference level (no flow) and $f(t)$ is a time-dependent forcing, e.g. due to changes in SPCZ location and intensity, in our case. Because oxygen isotopes are stable, their concentration in the aquifer model is simply a function of variations in the level of water, so $\delta^{18}O$ calcite is assumed to be proportional to $h$. In using $\delta^{18}O$

calcite as a proxy for precipitation amount, we are making a number of assumptions:

- calcite formation occurs at equilibrium, so $\delta^{18}O$ of calcite is representative of $\delta^{18}O$ of dripwater
- the aquifer is well-mixed, so $\delta^{18}O$ dripwater is representative of $\delta^{18}O$ rainfall
- $\delta^{18}O$ of rainfall is primarily governed by variations in precipitation amount (the "amount effect")

If these assumptions hold, then the measured $\delta^{18}O$ calcite is inversely related to the amount of water being delivered to the stalagmite (dilution effect in the model driven by the amount effect above-ground), which we assume to be a linear function of $h$ on the timescales of interest here (annual and longer). Thus, using $\delta^{18}O$ calcite as a proxy for rainfall amount amounts to back out $f(t)$ from $h$ using (1). Because the problem is (in this simplified case) linear, the general solution to the problem can be written as the convolution of the Green's function $g(t)$ with the forcing $f(t)$:

$$h(t) = g * f = \int_0^\infty f(\tau) g(t-\tau) d\tau \quad (2)$$

Conversely, the task of backing out $f(t)$ from measurements of $h(t)$ is a classic **deconvolution problem**. The Green's function (the system's response to an impulse forcing at $t = 0$) for this elementary problem is well known:

$$g(t) = H(t) \frac{1}{\phi} e^{-t/\tau_h} \quad (3)$$

Where *H* is the Heaviside switch. That is, for all positive times, the solution is a decaying exponential with an **e**-folding time $\tau_h = \frac{\phi}{a}$, called the aquifer recharge time*(24)*. The aquifer thus acts as an integrator of the climate forcing. To see this, consider the transfer function $\tilde{g}(\omega)$ (the Green's function Fourier transform):

$$\tilde{g} \propto \frac{1}{\gamma_h + i\omega} \quad (4)$$

where $\gamma_h = \tau_h^{-1}$ is the recharge rate. Now consider the extreme case of a white noise climate forcing ($\tilde{f} = 1$). In this case, the speleothem $\delta^{18}O$ spectrum would be proportional to $\left|\tilde{g}(\omega)\right|^2 \propto \frac{1}{\gamma_h^2 + \omega^2}$: that is, a pure red noise spectrum. In other words, the karst's effect is to exaggerate low-frequency variability at the expense of high-frequency variability. The resultant stalagmite $\delta^{18}O$ timeseries therefore exaggerates decadal and multi-decadal power at the expense of interannual power. How does aquifer recharge time influence the inference made from isotopic measurements in the calcite about the climate? This question is explored in Figure S10. It is apparent that a short recharge time (6 months) distorts the original signal very little, so the cyan curve is very close to the gray curve. However, a long recharge time (4 years) introduces much persistence, so removing it via deconvolution yields a much flatter spectrum. In other words, the longer the aquifer recharge time, the more pronounced the exaggeration. However, in all cases the multi-decadal peak stands out as significant with respect to red noise. Our current knowledge of the karst does not allow this value to be experimentally constrained,

but an argument can be made that its value must lie in the range [0.5 to 4]. Although this value controls the relative magnitude of multi-decadal to interannual power that we infer about climate, the dynamics captured by this simple model cannot, by themselves, produce such a peak. For any reasonable choice of values, the peak ca. 50 years would therefore be a salient feature of the input climate, and would likely require a dynamical explanation in terms of SPCZ intensity and/or location. It cannot, by itself, arise from karst dynamics.

**Correlation between Stalagmite $\delta^{18}O$ and Solar Reconstructions**

To quantify possible links between solar forcing and our rainfall proxy, we calculate the correlation between stalagmite $\delta^{18}O$ variations and three different reconstructions (Wang et al., 2005; Steinhilber et al., 2009; Vieira et al., 2011) of solar variability at various solar periodicities (11, 88, and 205 years) (Gray et al., 2010) and the dominant periodicity in our stalagmite record (~50 years) (See Table S2). Three independent reconstructions are used as each contains fairly large uncertainties (Schmidt et al., 2011). Two of the reconstructions use cosmogenic isotopes to estimate low-frequency variations in solar activity (Steinhilber et al., 2009; Vieira et al., 2011), while the Wang et al. (2005) reconstruction uses only astronomical observations. In addition, the Wang et al., (2005) dataset includes a reconstruction of the 11-year Schwabe cycle. Correlations (r) are calculated on wavelet-filtered timeseries, while *p*-values are estimated via a non-parametric test (Ebisuzaki, 1997) that corrects for the loss of degrees of freedom due to filtering.

The percentage of variance accounted for by each frequency band is calculated using Singular Spectrum Analysis in the kSpectra software package.

Table S2 shows that the only significant correlations ($p < 0.05$) occur at the Gleissberg cycle (88 years) between the stalagmite record and the Wang et al. (2005) and the Steinhilber et al. (2009) reconstructions. All other correlations are statistically insignificant at the 5% level. Despite this significance, the 80-100 year period accounts for less than 0.01% of the variance in the stalagmite $\delta^{18}O$ record, so the Gleissberg cycle is at best a very minor source of variability in our rainfall record. We conclude that there is no discernible influence of solar variability on our reconstructed record of SPCZ rainfall.

**Author Contributions.** J.W.P. wrote the manuscript, wrote the Matlab script for the age model, and prepared all figures and supplementary info, T.M.Q. provided analytical funding support, J.W.P, T.M.Q., J.E.G. and C.C.S assisted with the interpretation of the data and with manuscript preparation, C.C.S and K.L. measured U-Th ages, F.W.T. provided funding for field support, C.R.M. made $\delta^{18}O$ measurements and assisted with the interpretation of the data, C.S.J. and J.E.G. provided valuable advice on statistical matters and input on climatic interpretations as well as helping with manuscript preparation, J.E.G. calculated the MTM and wavelet spectra, tested for significance, and performed the karst hydrology calculation, J.L.B. provided funding for field support, D.J.S. discovered the field-site, collected and cataloged the stalagmite sample, ran pilot geochemical analyses and preliminary dating, C.A.H. measured Pb-210 ages. All authors provided input on the final version of the manuscript.

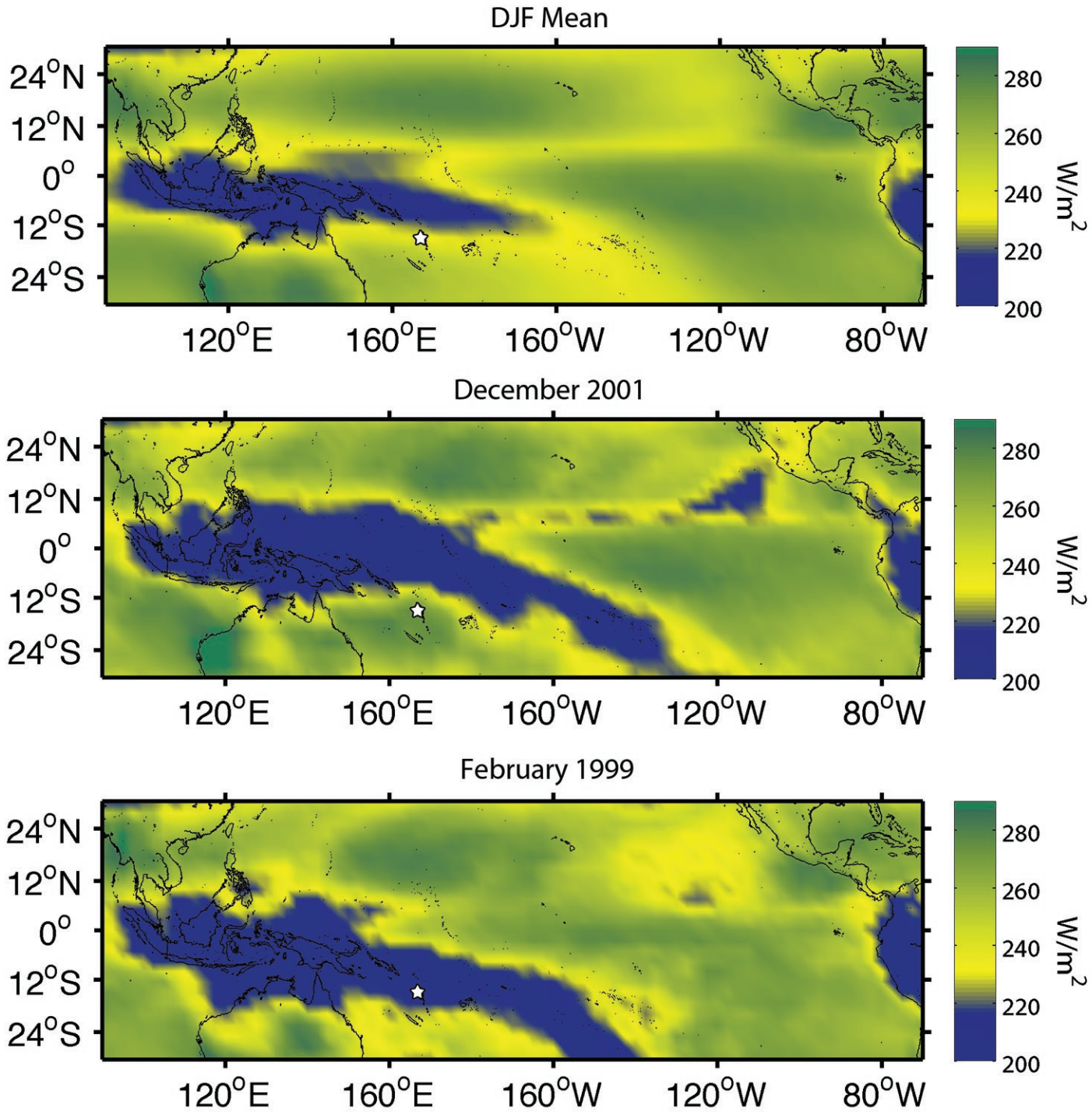


Figure S1 | OLR plots for the composite of DJF (1974-2011) (top), December 2001 (middle) when the SPCZ is fully formed and is shifted to the northeast, and February 1999 (bottom) when the SPCZ is fully formed and is shifted to the southwest. OLR is a proxy for cloud top temperature and consequently rainfall. Lower values of OLR indicate colder temperatures that result from deep convection/higher rainfall. When the SPCZ is to the NE, it is not over Vanuatu (white star) as in Dec. 2001. When the SPCZ is to the SW, it is over Vanuatu (white star) as in Feb. 1999.

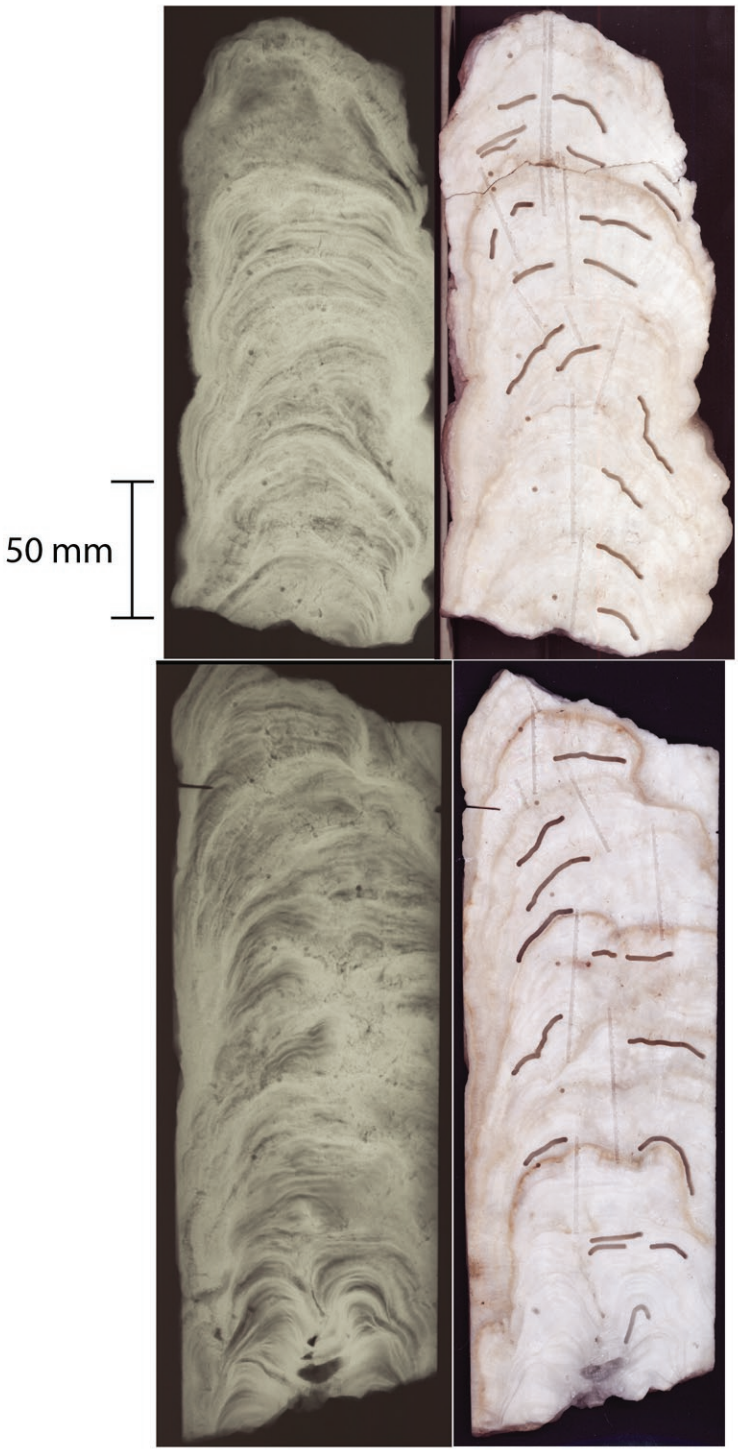


Figure S2 | X-ray and visible scans of stalagmite Big Taurius from Taurius Cave, Espiritu Santo, Vanuatu. Long, deep troughs which are drilled along a growth layer (left to right) represent samples taken for U-Th dating. Only a subset of the dates drilled is depicted in the scan. Small, shallow troughs along the growth axis (up and down) represent samples taken for isotopic analysis. Examples of parallel paths that overlap between the middle and sides are plotted in Figure S7 as part of the Hendy Test to demonstrate internal reproducibility.

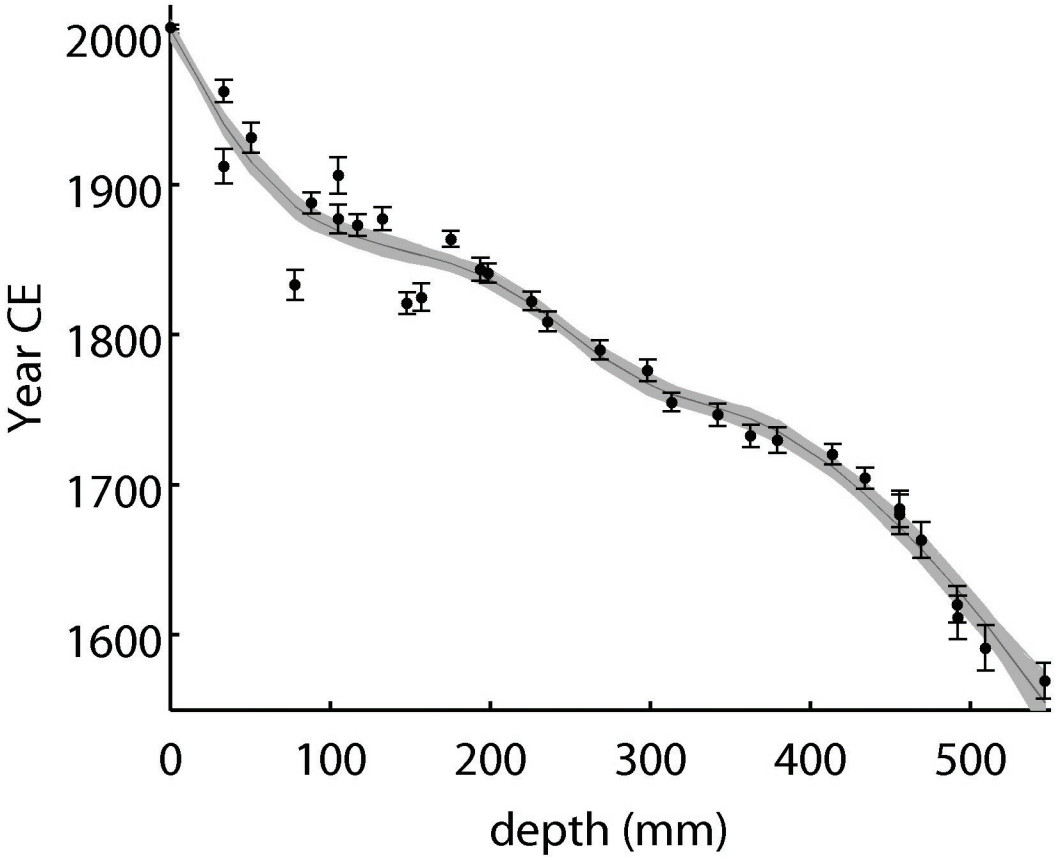


Figure S3 | Age model for sample Big Taurius based on 31 U-Th ages, and an age constraint where the top is assumed to be c. 2005 (year of collection). The dark curve in the middle of the grey spread represents the median age model. The 10,000 Monte Carlo iterations of alternate age models are plotted in grey.

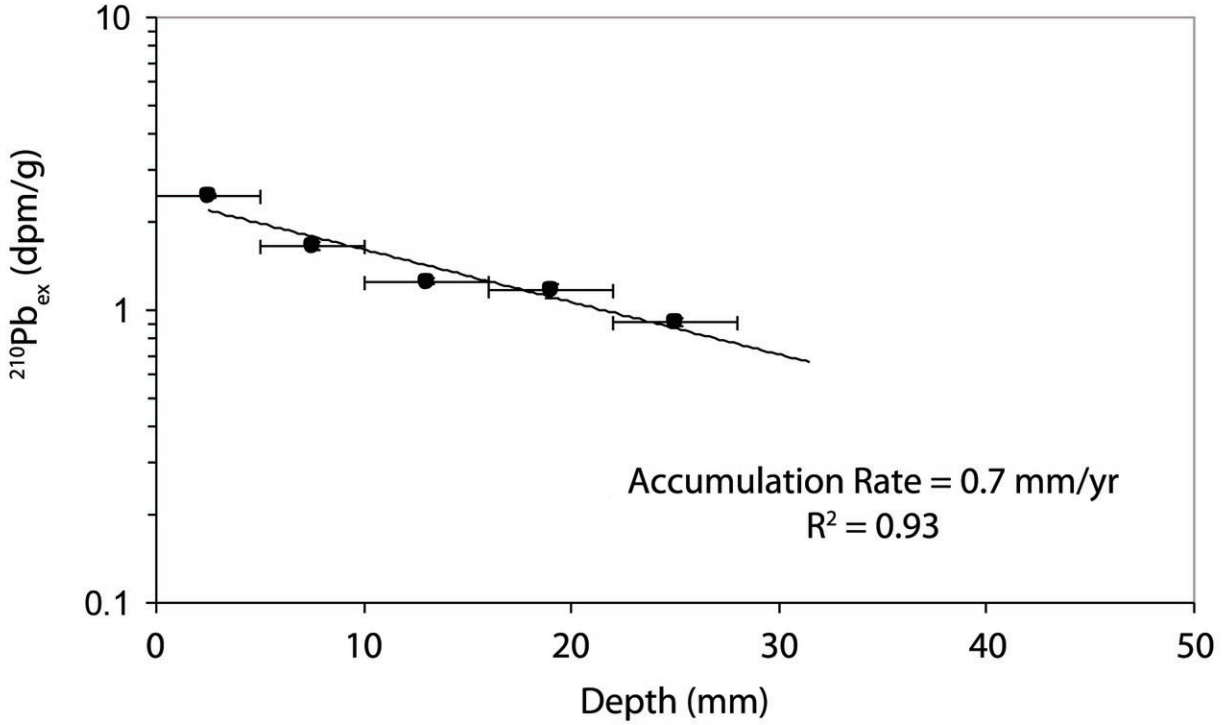


| Depth (mm) | | $^{210}Pb_{ex}$ |
|---|---|---|
| Top | Bottom | (dpm/g) |
| 0 | 5 | 2.456 ± 0.044 |
| 5 | 10 | 1.660 ± 0.056 |
| 10 | 16 | 1.250 ± 0.027 |
| 16 | 22 | 1.163 ± 0.069 |
| 22 | 28 | 0.905 ± 0.029 |

Figure S4 | Lead-210 dating of the top of the stalagmite. The calculated growth-rate via Lead-210 equals the estimate of the U-Th dates. Both dating techniques capture the relatively slower rate at the top of ~0.6-0.7 mm/year.

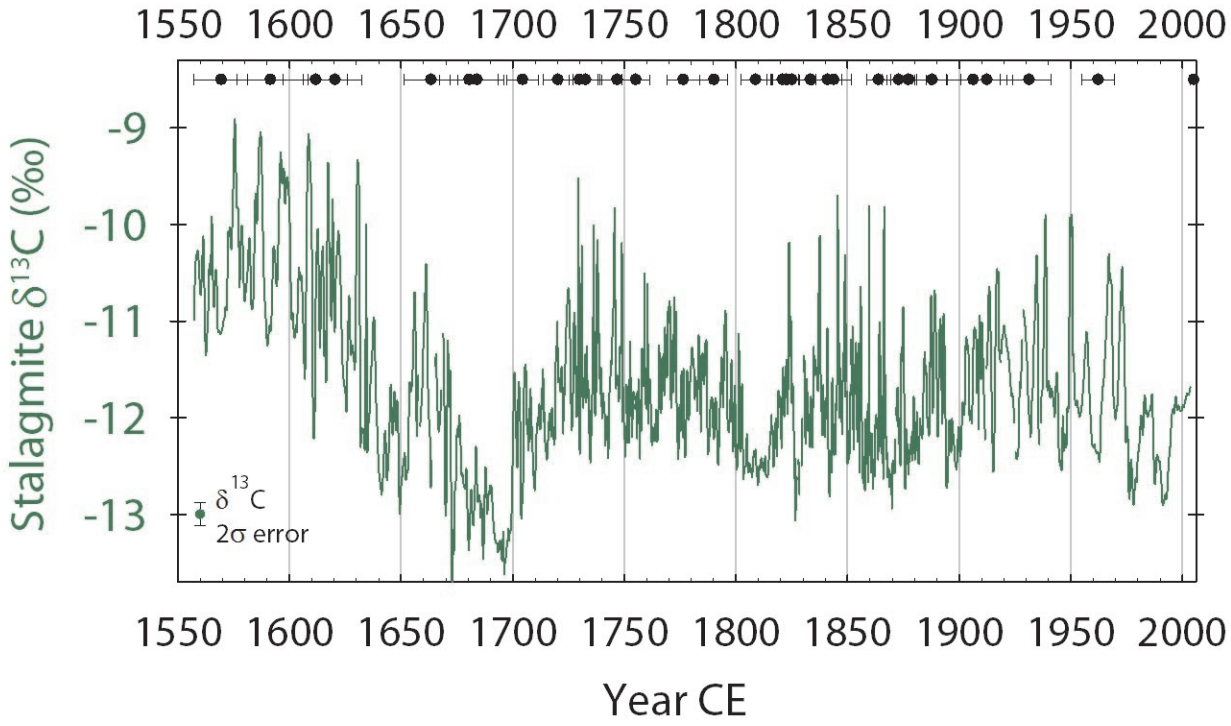


Figure S5 | Timeseries of $\delta^{13}C$ for stalagmite sample Big Taurius. U-Th dates are plotted along the top as in Figure 2a for $\delta^{18}O$. The carbon timeseries contains little of the 50-year periodicity found in the $\delta^{18}O$ record and is mostly characterized by high frequency and centennial-scale variability most likely linked to the strong annual cycle in rainfall as well as ENSO events on interannual timescales.

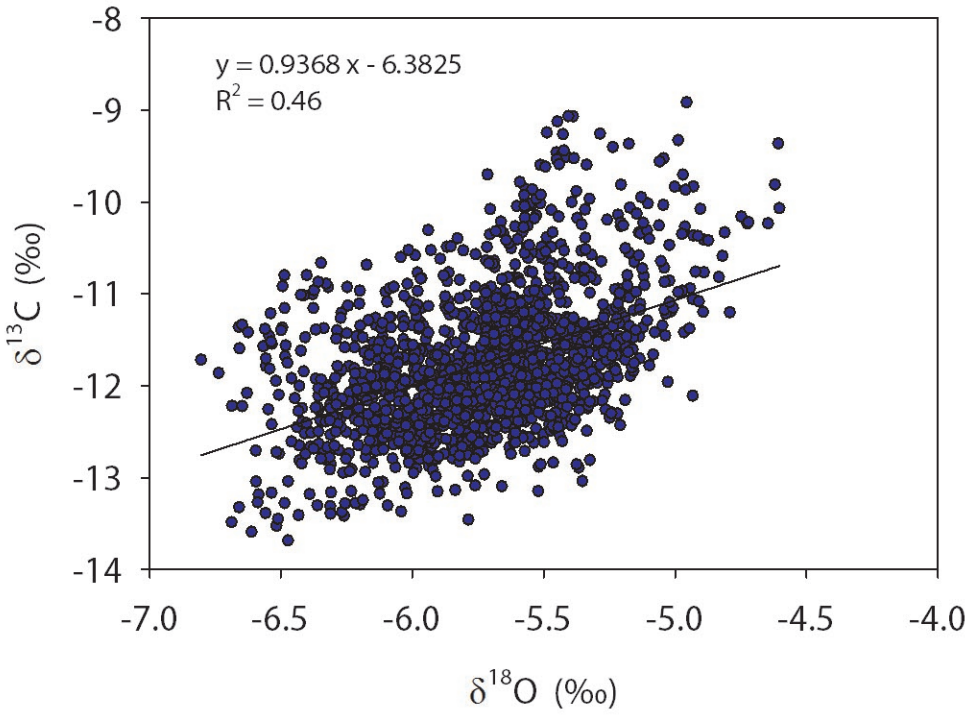


Figure S6 | Cross-plot of $\delta^{18}O$ vs $\delta^{13}C$ as part of a Hendy test. While the two timeseries share approximately 50% of their variance, it is driven mainly by the annual cycle in rainfall and interannual variability during ENSO events. A visual comparison of the individual timeseries (Figure 2a and S5) reveals that there is no correlation on multi-decadal timescales between $\delta^{18}O$ and $\delta^{13}C$. Therefore, the multi-decadal periodicity in $\delta^{18}O$ is most likely due to changes in rainfall $\delta^{18}O$ (a proxy for rainfall amount) and not due to kinetic effects (Hendy, 1971; Mickler et al., 2004; Mickler et al., 2006; Dorale and Liu, 2009).

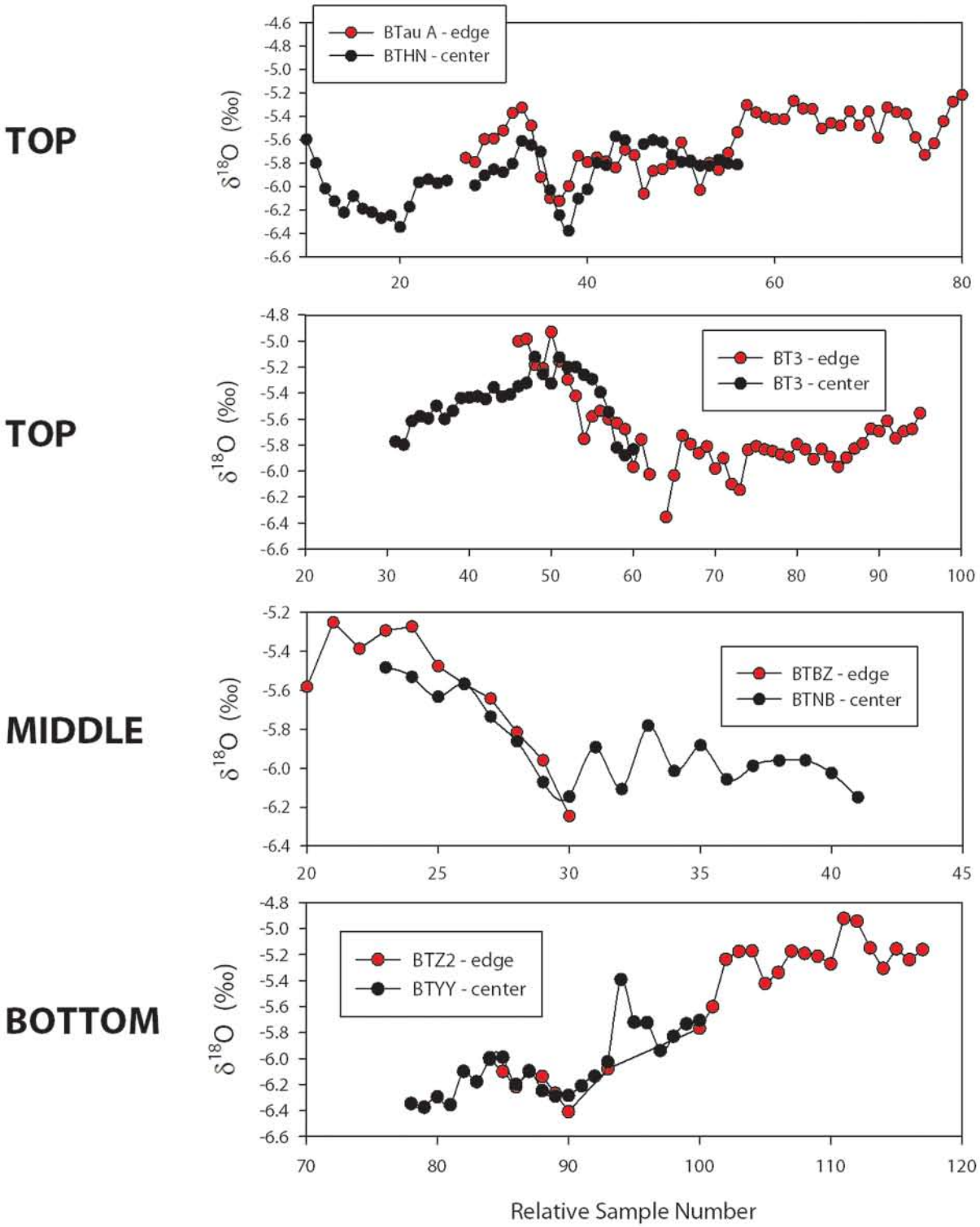


Figure S7 | Stalagmite $\delta^{18}O$ as a function of distance from the center growth axis as part of the Hendy Test for four regions of the sample. Unlike a more traditional Hendy test where a series of samples are drilled across a growth layer (that may or may not contain contemporaneous powder), overlapping paths that are used in the final $\delta^{18}O$ timeseries are plotted a function of relative sample number. As bands are not perfectly parallel and tend to pinch and spread out in a stalagmite, the individual samples do not have the same temporal resolution. There is no consistent progressive enrichment of $\delta^{18}O$ from the center of the sample to the edges supporting the conclusion that kinetic effects do not play a major role in governing the isotopic composition of the stalagmite.

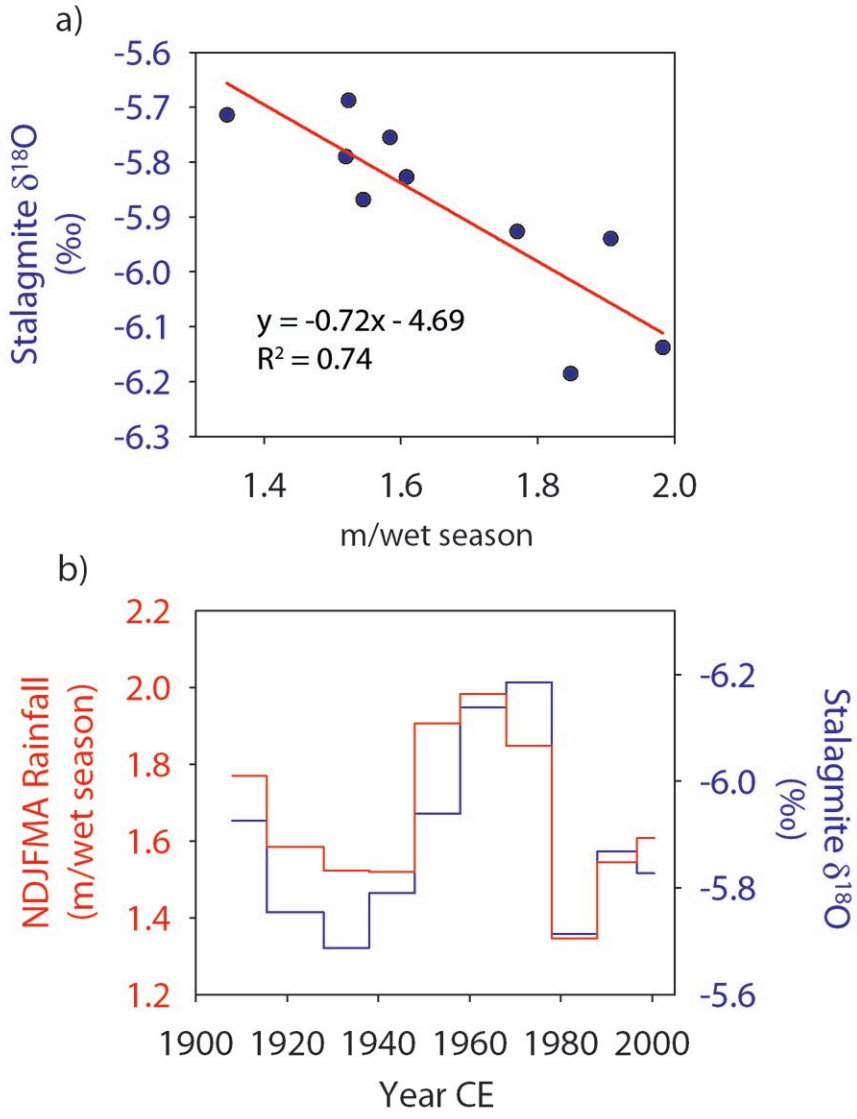


Figure S8 | a) Crossplot of decadal averages of stalagmite $\delta^{18}O$ from Taurius Cave, Espiritu Santo, Vanuatu and wet season rainfall from Pekoa Airport, Espiritu Santo, Vanuatu (~20 km apart) to quantify the inverse relationship known as the "Amount Effect". The slope of the linear regression estimates that a change of 0.72‰ in stalagmite $\delta^{18}O$ equals approximately 1 m/wet season of rainfall change, or equivalently 1‰ stalagmite $\delta^{18}O$ for every 1.4 m/wet season of rainfall. b) Timeseries of the decadal averages of stalagmite $\delta^{18}O$ and wet season rainfall from Pekoa Airport showing the amount effect relationship. Note the inverted axis for stalagmite $\delta^{18}O$.

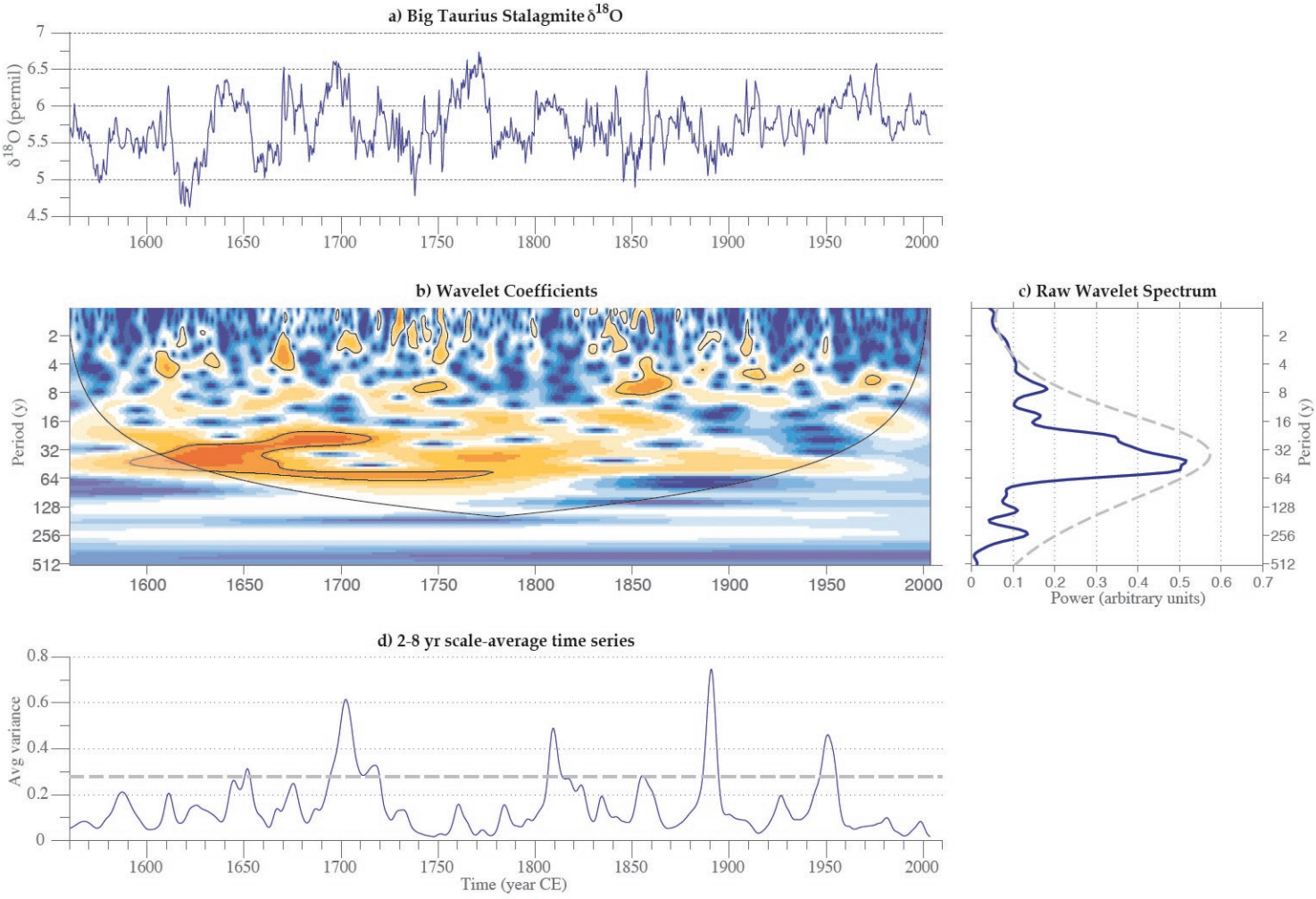


Figure S9 | Morlet wavelet spectrum (Torrence and Compo, 1998; Liu et al., 2007) for the Big Taurius $\delta^{18}O$ timeseries. a) Original stalagmite $\delta^{18}O$ timeseries. b) Wavelet spectrum, where orange colors represent higher power and black contours represent the AR(1) 95% confidence level. c) Global wavelet spectrum where the dashed grey line is the AR(1) 95% confidence level. d) Average variance in the 2-8 year scale-average timeseries where the grey line is the AR(1) 95% confidence level. Much of the timeseries displays significant variability at multi-decadal as well as interannual (2-8 year) periodicities (b). However, there is a noticeable lack of power at the 11-year period overall, and in the 2-8 year band over the last 100 years, most likely due to the reduction in growth rate during this interval, which hampers calibration efforts with instrumental variables like the Niño 3.4 index.

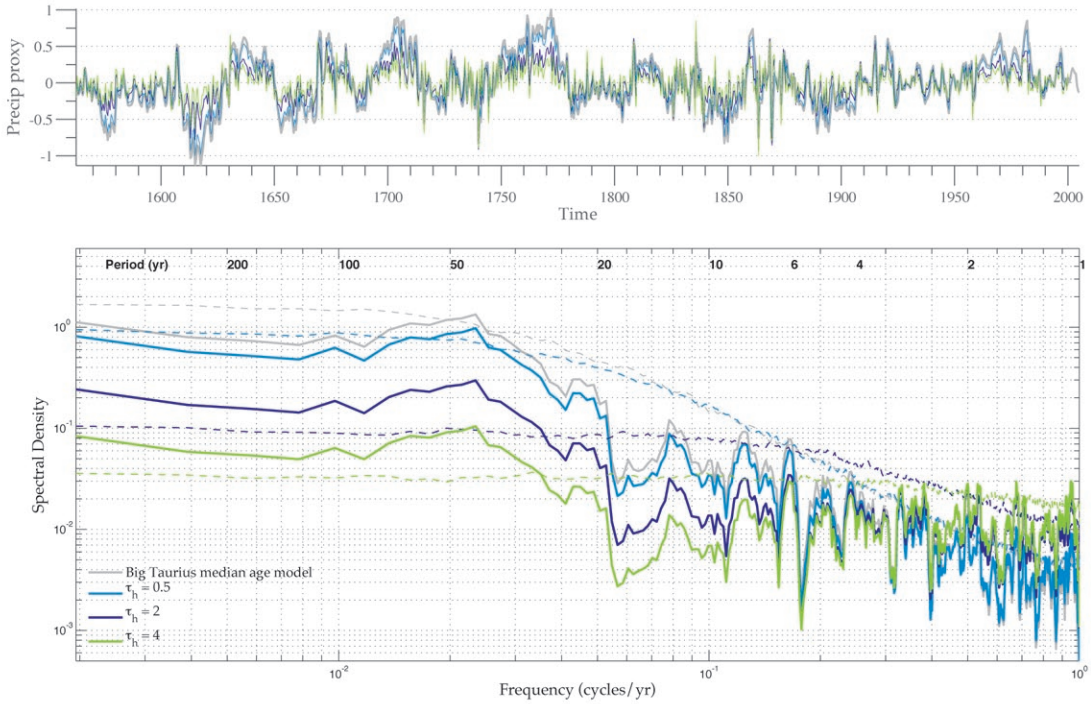


Figure S10 | Effect of deconvolution for 3 values of the aquifer recharge parameter $\tau_h$. Top: isotopic signal at Big Taurius using the median age model interpolated at regular increments of 6 months (gray) and deconvolved aquifer forcings (rainfall) for $\tau_h$ = 0.5, 1 and 2 years, respectively. Bottom: MTM spectral density of those signals. Dashed lines represent the 95% quantile based on the spectra of 200 realizations of an AR(1) process fitted to each series. Peaks surpassing the dashed curves of the same color can therefore be deemed significant at the 5% level.

Table S1 | MC-ICP-MS U-Th data table

| Depth (mm) | Chemistry perfomed on | Sample ID | Weight (g) | $^{238}U$ (ppb) | $^{232}Th$ (ppt) | $\delta^{234}U$ measured[a] | $[^{230}Th/^{238}U]$ activity[c] | $[^{230}Th/^{232}Th]$ (ppm)[d] | Age uncorrected | Age corrected [c,e] | $\delta^{234}U_{initial}$ corrected[b] | Year CE |
|---|---|---|---|---|---|---|---|---|---|---|---|---|
| 33.4 | 4/13/09 | t2 | 0.20053 | 191.4 ± 1.1 | 23.5 ± 3.5 | 96.4 ± 5.6 | 0.0005018 ± 0.000073 | 67 ± 14 | 50.0 ± 7.3 | 47.0 ± 7.5 | 96.4 ± 5.6 | 1962.2 ± 7.5 |
| 33.4 | 4/13/09 | t1 | 0.29566 | 145.66 ± 0.74 | 79.0 ± 2.4 | 101.2 ± 4.5 | 0.001108 ± 0.00010 | 33.7 ± 3.1 | 110 ± 10 | 97 ± 12 | 101.2 ± 4.5 | 1912.4 ± 11.6 |
| 50.5 | 4/21/11 | M2 | 0.20380 | 145.96 ± 0.35 | 74.2 ± 3.4 | 99.9 ± 3.2 | 0.0009267 ± 0.000081 | 30.1 ± 3.0 | 92.0 ± 8.1 | 80 ± 10 | 99.9 ± 3.2 | 1931.3 ± 10.0 |
| 77.9 | 4/21/11 | M3 | 0.17780 | 184.68 ± 0.43 | 40.2 ± 3.9 | 101.5 ± 3.1 | 0.001849 ± 0.00010 | 140 ± 15 | 183 ± 10 | 178 ± 10 | 101.6 ± 3.1 | 1833.3 ± 10.0 |
| 88.2 | 4/28/10 | BT-12 | 0.67201 | 198.07 ± 0.28 | 32.9 ± 1.1 | 98.5 ± 1.7 | 0.0012689 ± 0.000067 | 126.2 ± 7.8 | 126.2 ± 6.6 | 122.2 ± 6.9 | 98.5 ± 1.7 | 1887.8 ± 6.9 |
| 104.9 | 4/28/10 | BT-13a | 0.67433 | 213.42 ± 0.33 | 34.4 ± 1.1 | 96.3 ± 2.0 | 0.001371 ± 0.00010 | 140 ± 11 | 136.7 ± 9.5 | 133 ± 10 | 96.3 ± 2.0 | 1877.2 ± 9.7 |
| 104.9 | 4/28/10 | BT-13b | 0.31130 | 211.32 ± 0.29 | 32.8 ± 2.3 | 95.8 ± 1.8 | 0.001079 ± 0.00012 | 115 ± 15 | 108 ± 12 | 104 ± 12 | 95.8 ± 1.8 | 1906.2 ± 12.0 |
| 117.0 | 3/8/11 | 3 | 0.24512 | 159.64 ± 0.26 | 44.4 ± 3.0 | 97.5 ± 2.5 | 0.0014579 ± 0.000064 | 86.5 ± 7.0 | 145.1 ± 6.4 | 138.4 ± 7.2 | 97.6 ± 2.5 | 1872.9 ± 7.2 |
| 132.6 | 4/28/10 | BT-14 | 0.80609 | 172.76 ± 0.20 | 29.03 ± 0.89 | 97.2 ± 1.6 | 0.0013728 ± 0.000076 | 134.9 ± 8.5 | 136.7 ± 7.6 | 132.7 ± 7.9 | 97.3 ± 1.6 | 1877.3 ± 7.9 |
| 147.9 | 3/8/11 | 4 | 0.20785 | 197.53 ± 0.50 | 76.2 ± 3.4 | 98.6 ± 2.9 | 0.0020072 ± 0.000056 | 85.9 ± 4.5 | 199.7 ± 5.6 | 190.4 ± 7.3 | 98.6 ± 2.9 | 1820.9 ± 7.3 |
| 156.8 | 4/28/10 | BT-15 | 0.51554 | 145.90 ± 0.2 | 38.8 ± 1.4 | 95.9 ± 1.8 | 0.0019200 ± 0.000085 | 119.1 ± 6.7 | 191.4 ± 8.5 | 185.0 ± 9.1 | 95.9 ± 1.8 | 1914.1 ± 9.1 |
| 175.3 | 4/21/11 | M6 | 0.24830 | 317.07 ± 0.66 | 41.8 ± 2.8 | 95.0 ± 2.7 | 0.0015104 ± 0.000051 | 189 ± 14 | 150.7 ± 5.1 | 147.5 ± 5.4 | 95.0 ± 2.7 | 1863.8 ± 5.4 |
| 193.8 | 4/21/11 | M7 | 0.15730 | 192.03 ± 0.41 | 24.7 ± 4.4 | 97.4 ± 2.5 | 0.0017141 ± 0.000077 | 220 ± 41 | 170.7 ± 7.7 | 167.6 ± 7.8 | 97.5 ± 2.5 | 1843.7 ± 7.8 |
| 198.4 | 3/8/11 | 6 | 0.27277 | 214.99 ± 0.82 | 33.9 ± 3.2 | 101.1 ± 4.9 | 0.0017542 ± 0.000060 | 184 ± 19 | 174.1 ± 6.0 | 170.3 ± 6.3 | 101.1 ± 4.9 | 1841.0 ± 6.3 |
| 225.8 | 3/8/11 | 7 | 0.21657 | 180.39 ± 0.38 | 41.3 ± 2.6 | 99.7 ± 2.8 | 0.0019553 ± 0.000054 | 141 ± 10 | 194.3 ± 5.4 | 188.8 ± 6.0 | 99.7 ± 2.8 | 1822.5 ± 6.0 |
| 235.8 | 3/8/11 | 8 | 0.2037 | 199.20 ± 0.42 | 70.7 ± 2.8 | 98.1 ± 2.7 | 0.0021209 ± 0.000051 | 98.6 ± 4.6 | 211.1 ± 5.1 | 202.6 ± 6.7 | 98.1 ± 2.7 | 1808.7 ± 6.7 |
| 268.5 | 4/28/10 | BT-10 | 0.70014 | 196.47 ± 0.28 | 24.9 ± 1.0 | 97.6 ± 1.8 | 0.0022391 ± 0.000062 | 292 ± 14 | 223.0 ± 6.2 | 219.9 ± 6.4 | 97.7 ± 1.8 | 1790.1 ± 6.4 |
| 298.3 | 3/8/11 | 11 | 0.2817 | 154.19 ± 0.46 | 43.9 ± 1.9 | 98.9 ± 3.9 | 0.0024306 ± 0.000063 | 140.8 ± 7.2 | 241.8 ± 6.4 | 234.9 ± 7.2 | 98.9 ± 3.9 | 1776.4 ± 7.2 |
| 313.3 | 4/28/10 | BT-9 | 0.47533 | 249.12 ± 0.27 | 46.2 ± 1.5 | 96.5 ± 1.7 | 0.0026018 ± 0.000059 | 231.7 ± 9.1 | 259.4 ± 5.9 | 254.9 ± 6.3 | 96.6 ± 1.7 | 1755.1 ± 6.3 |
| 342.1 | 3/8/11 | 13 | 0.23202 | 150.55 ± 0.45 | 38.6 ± 1.5 | 95.3 ± 4.2 | 0.0027124 ± 0.000068 | 174.8 ± 8.1 | 270.8 ± 6.9 | 264.6 ± 7.5 | 95.3 ± 4.2 | 1746.7 ± 7.5 |
| 362.7 | 4/28/10 | BT-6 | 0.71766 | 221.40 ± 0.25 | 40.9 ± 1.0 | 96.7 ± 1.6 | 0.0028276 ± 0.000070 | 252.6 ± 8.7 | 281.9 ± 7.0 | 277.4 ± 7.4 | 96.8 ± 1.6 | 1732.6 ± 7.4 |
| 379.4 | 3/8/11 | 14 | 0.2804 | 185.43 ± 0.58 | 60.5 ± 3.0 | 98.4 ± 4.8 | 0.0029063 ± 0.000074 | 147.1 ± 8.2 | 289.3 ± 7.5 | 281.4 ± 8.4 | 98.5 ± 4.8 | 1729.9 ± 8.4 |
| 413.9 | 4/28/10 | BT-8 | 0.39023 | 261.37 ± 0.61 | 34.2 ± 1.8 | 96.2 ± 3.1 | 0.0029363 ± 0.000065 | 371 ± 21 | 292.9 ± 6.6 | 289.7 ± 6.8 | 96.3 ± 3.1 | 1720.3 ± 6.8 |
| 434.2 | 3/8/11 | 15 | 0.24205 | 258.05 ± 0.63 | 20.0 ± 2.7 | 98.1 ± 3.6 | 0.0031009 ± 0.000070 | 659 ± 90 | 308.8 ± 7.0 | 306.9 ± 7.1 | 98.2 ± 3.6 | 1704.4 ± 7.1 |
| 455.9 | 4/13/09 | b1 | 0.31730 | 147.38 ± 0.85 | 50.0 ± 2.2 | 98.1 ± 5.9 | 0.003384 ± 0.00012 | 164.7 ± 9.4 | 337 ± 13 | 329 ± 13 | 98.1 ± 5.9 | 1680.4 ± 13.2 |
| 455.9 | 4/13/09 | b2 | 0.38405 | 131.91 ± 0.56 | 39.4 ± 1.8 | 98.7 ± 4.5 | 0.003341 ± 0.00011 | 185 ± 11 | 332 ± 11 | 325 ± 12 | 98.8 ± 4.5 | 1683.9 ± 12.0 |
| 469.4 | 4/21/11 | M8 | 0.23210 | 111.14 ± 0.18 | 50.8 ± 3.0 | 95.5 ± 2.1 | 0.003600 ± 0.00010 | 130.0 ± 8.5 | 359 ± 10 | 348 ± 12 | 95.5 ± 2.1 | 1663.3 ± 12.0 |
| 491.8 | 4/21/11 | M9 | 0.25350 | 147.83 ± 0.25 | 27.7 ± 2.7 | 96.7 ± 2.3 | 0.003967 ± 0.00012 | 350 ± 36 | 396 ± 12 | 391 ± 12 | 96.8 ± 2.3 | 1620.3 ± 12.0 |
| 492.2 | 3/8/11 | 16 | 0.31309 | 232.69 ± 0.77 | 21.9 ± 1.9 | 92.7 ± 5.1 | 0.004015 ± 0.00014 | 705 ± 65 | 402 ± 14 | 400 ± 14 | 92.8 ± 5.1 | 1611.7 ± 14.3 |
| 509.6 | 4/21/11 | M10 | 0.17530 | 94.96 ± 0.10 | 25.9 ± 4.0 | 96.9 ± 1.9 | 0.004279 ± 0.00014 | 259 ± 41 | 427 ± 14 | 420 ± 15 | 97.0 ± 1.9 | 1591.3 ± 15.0 |
| 546.6 | 4/21/11 | M11 | 0.18560 | 124.35 ± 0.19 | 32.9 ± 3.8 | 98.7 ± 2.2 | 0.004503 ± 0.00011 | 281 ± 33 | 448 ± 11 | 442 ± 12 | 98.8 ± 2.2 | 1569.3 ± 12.0 |

Analytical errors are 2σ of the mean.

[a] $\delta^{234}U = ([^{234}U/^{238}U]_{activity} - 1) \times 1000$.

[b] $\delta^{234}U_{initial}$ corrected was calculated based on $^{230}Th$ age (T), i.e., $\delta^{234}U_{initial} = \delta^{234}U_{measured} X e^{\lambda_{234} T}$, and T is corrected age.

[c] $[^{230}Th/^{238}U]_{activity} = 1 - e^{-\lambda_{230} T} + (\delta^{234}U_{measured}/1000)[\lambda_{230}/(\lambda_{230} - \lambda_{234})](1 - e^{-(\lambda_{230} - \lambda_{234}) T})$, where $T$ is the age.

Decay constants are 9.1577 x $10^{-6}$ $yr^{-1}$ for $^{230}Th$, 2.8263 x $10^{-6}$ $yr^{-1}$ for $^{234}U$ (Cheng et al., 2000), and 1.55125 x $10^{-10}$ $yr^{-1}$ for $^{238}U$ (Jeffey et al., 1971) .

[d] The degree of detrital $^{230}Th$ contamination is indicated by the $[^{230}Th/^{232}Th]$ atomic ratio instead of the activity ratio.

[e] Age corrections were calculated using an estimated atomic $^{230}Th/^{232}Th$ ratio of 4 ± 2 ppm.

Table S2 | Correlation of Vanuatu Stalagmite $\delta^{18}O$ with Solar Reconstructions

Vieira et al., (2011) Reconstruction

| Period | % Variance in Stal $\delta^{18}O$ | % Variance in Solar Recon | r | p |
|---|---|---|---|---|
| 9-13 years | 6% | <0.01 | -0.05 | 0.73 |
| 40-50 years | 50% | 3% | 0.10 | 0.76 |
| 80-100 years | < 0.01% | 16% | -0.63 | 0.14 |
| 180-220 years | < 0.01% | 47% | -0.44 | 0.66 |

Steinhilber et al., (2009) Reconstruction

| Period | % Variance in Stal $\delta^{18}O$ | % Variance in Solar Recon | r | p |
|---|---|---|---|---|
| 9-13 years | 6% | <0.01 | 0.04 | 0.71 |
| 40-50 years | 50% | 2% | 0.43 | 0.12 |
| 80-100 years | < 0.01% | 11% | -0.74 | 0.02 |
| 180-220 years | < 0.01% | 86% | -0.48 | 0.66 |

Wang et al., (2005) Reconstruction

| Period | % Variance in Stal $\delta^{18}O$ | % Variance[†] in Solar Recon | r | p |
|---|---|---|---|---|
| 9-13 years | 6% | 18% | -0.12 | 0.54 |
| 40-50 years | 50% | 2% | 0.29 | 0.35 |
| 80-100 years | < 0.01% | 10% | -0.84 | <0.001 |
| 180-220 years | < 0.01% | 60% | -0.49 | 0.64 |

Correlations (r) and p-values are calculated on wavelet-filtered timeseries for the specified periods.

Percent variance is calculated using Singular Spectrum Analysis in the kSpectra software package. Window length = 50 years.

[†] For the Lean reconstruction, percent variance and correlations are for 1610-2000 CE.

## SI References


Dansgaard, W., 1964. Stable isotopes in precipitation. Tellus. v. 16, p. 436-468.

Dorale, J. A., and Liu, Z. H., 2009. Limitations of Hendy Test Criteria in Judging the Paleoclimatic Suitability of Speleothems and the Need for Replication. J. Cave Karst Stud. v. 71, p. 73-80.

Ebisuzaki, W., 1997. A method to estimate the statistical significance of a correlation when the data are serially correlated. J. Clim. v. 10, p. 2147-2153.

Gelhar, L. W., and Wilson, J. L., 1974. Ground-water quality modeling. Ground Water. v. 12, p. 399-408.

Gray, L. J., et al., 2010. Solar Influences on Climate. Reviews of Geophysics. v. 48, p.

Hendy, C. H., 1971. Isotopic geochemistry of speleothems .1. Calculation of effects of different modes of formation on isotopic composition of speleothems and their applicability as palaeoclimatic indicators. Geochim. Cosmochim. Acta. v. 35, p. 801-824.

Huh, C. A., Small, L. F., Niemnil, S., Finney, B. P., Hickey, B. M., Kachel, N. B., Gorsline, D. S., and Williams, P. M., 1990. Sedimentation dynamics in the Santa Monica-San Pedro Basin off Los Angeles: radiochemical, sediment trap and transmissometer studies. Continental Shelf Research. v. 10, p. 137-164.

MacClancy, J., 1981. To Kill a Bird with Two Stones: A Short History of Vanuatu. Port Vila, Vanuatu Cultural Centre Publications.

Mickler, P. J., Banner, J. L., Stern, L., Asmerom, Y., Edwards, R. L., and Ito, E., 2004. Stable isotope variations in modern tropical speleothems: Evaluating equilibrium vs. kinetic isotope effects. Geochim. Cosmochim. Acta. v. 68, p. 4381-4393.

Mickler, P. J., Stern, L. A., and Banner, J. L., 2006. Large kinetic isotope effects in modern speleothems. Geol. Soc. Am. Bull. v. 118, p. 65-81.

Partin, J. W., et al., 2012. Relationship between modern rainfall variability, cave dripwater, and stalagmite geochemistry in Guam, USA. Geochemistry Geophysics Geosystems. v. 13, p.

Paton, J. G., 1893. The Story of John G. Paton Told for Young Folks or Thirty Years among South Sea Cannibals. New York, American Tract Society.

Rozanski, K., Araguas-Araguas, L., and Gonfiantini, R., 1993. Isotopic patterns in modern global precipitation. Climate Change in Continental Isotopic Records. P. K. Swart, K. C. Lohmann, J. McKenzie and S. Savin. Washington, DC, American Geophysical Union**:** 1-36.

Schmidt, G. A., et al., 2011. Climate forcing reconstructions for use in PMIP simulations of the last millennium (v1.0). Geoscientific Model Development. v. 4, p. 33-45.

Shen, C. C., et al., 2012. High-precision and high-resolution carbonate Th-230 dating by MC-ICP-MS with SEM protocols. Geochim. Cosmochim. Acta. v. 99, p. 71-86.

Steinhilber, F., Beer, J., and Frohlich, C., 2009. Total solar irradiance during the Holocene. Geophys. Res. Lett. v. 36, p.

The_Lonely_Planet, 2012, "The Lonely Planet : Port Vila, Vanuatu - History." http://www.lonelyplanet.com/vanuatu/efate/port-vila/history (accessed May 2013).

Tremaine, D. M., Froelich, P. N., and Wang, Y., 2011. Speleothem calcite farmed in situ: Modern calibration of delta(18)O and delta(13)C paleoclimate proxies in a continuously-monitored natural cave system. Geochim. Cosmochim. Acta. v. 75, p. 4929-4950.

Vieira, L. E. A., Solanki, S. K., Krivova, N. A., and Usoskin, I., 2011. Evolution of the solar irradiance during the Holocene. Astronomy & Astrophysics. v. 531, p.

Wang, Y. M., Lean, J. L., and Sheeley, N. R., 2005. Modeling the sun's magnetic field and irradiance since 1713. Astrophysical Journal. v. 625, p. 522-538.